



HAL
open science

Adhesion for Coatings

E. Breton, Marie-Christine Baietto

► **To cite this version:**

E. Breton, Marie-Christine Baietto. Adhesion for Coatings. Science direct, 1992, 21 (C), pp.41-47.
10.1016/S0167-8922(08)70507-8 . hal-01951914

HAL Id: hal-01951914

<https://hal.science/hal-01951914v1>

Submitted on 6 Jul 2021

HAL is a multi-disciplinary open access archive for the deposit and dissemination of scientific research documents, whether they are published or not. The documents may come from teaching and research institutions in France or abroad, or from public or private research centers.

L'archive ouverte pluridisciplinaire **HAL**, est destinée au dépôt et à la diffusion de documents scientifiques de niveau recherche, publiés ou non, émanant des établissements d'enseignement et de recherche français ou étrangers, des laboratoires publics ou privés.



Distributed under a Creative Commons Attribution 4.0 International License

Adhesion for Coatings

E. Breton and M.-C. Dubourg

Spall detachment in coatings is modelled as a cracked coated medium submitted to contact loading. Few models analyse the role of interfacial cracks between coating and substrate. The existing models are limited in use, due to assumptions on number and location of displacement zones (stick, slip, open) along crack faces. Further only one crack is analysed at a time. A spall detachment is analysed as a combination of an interfacial crack that propagates at the interface and a surface breaking crack that propagates normally to the interface. These two cracks are analysed simultaneously. The energy release rate G is determined at crack tips. The method employed is half-analytical and half-numerical.

Results show that, for the case studied, crack interaction favours crack propagation. The following spall detachment process is proposed: the surface breaking crack propagates down to the interface and the interfacial crack propagates at the interface in a direction opposite to that of the load displacement.

1. Introduction

Spall detachment in coating is modelled as a cracked coated medium submitted to contact loading. Few papers consider the role of interfacial cracks between coating and substrate. Erdogan and Gupta [1, 2, 3], Farris and Keer [4] studied pressurized cracks between dissimilar materials. Stress intensity factors were calculated by Rice [5] for interfacial cracks. Kim and al [6] modelled interfacial crack behaviour with slip and stick zones under hertzian loading. These models are limited in use, due to assumptions on number and location of displacement zones (stick, slip, open) along crack faces. Further only one crack is analysed. A spall typical of those observed experimentally [7], is studied here. Spall detachment is the combination of an interfacial crack that propagates at the interface and a surface breaking crack that propagates normally to the interface. These two cracks are analysed simultaneously. The energy release rate G is determined at crack tips. The method employed is half analytical and half numerical. Cracks are modelled with continuous dislocation distributions [1, 2, 3]. Fourier integral

transforms techniques are used to obtain relations between stresses and dislocation distributions. These relations are integral equations solved following Erdogan and Gupta [3]. The contact problem between crack faces is then solved as an unilateral contact problem with friction [8].

Results show that crack interaction favours crack propagation. The following spall detachment process is proposed: the surface breaking crack propagates down to the interface and the interfacial crack propagates at the interface in a direction opposite to that of the load displacement.

2. Theory

The model determines the elastic energy release rate G for straight cracks situated in a loaded layered medium. G varies with the stress field σ^T at crack tip, which depends on the unknown distribution of displacement zones (open, stick, slip) along crack faces. σ^T is the combination of the continuum stress field σ^{MC} of the layered half-plane and of the crack field σ^F generated by displacement jumps along crack faces. Both stress fields σ^{MC} and σ^F must be

known to calculate G.

2.1 Assumptions

The cracked layered medium is modelled as a two-dimensional half-plane. Layer and substrate are homogeneous and isotropic. Linear elasticity conditions prevail. Normal $P(y)$ and tangential $Q(y)$ tractions are applied over the half-plane. Coulomb's law is considered ($Q(y) = f_s P(y)$). Friction between crack faces is taken account using Coulomb's law also. Load cycles are analysed using an incremental description of the load history as hysteresis is introduced by crack friction.

2.2 Continuous stress fields σ^{MC}

A thermomechanical multilayered model was developed earlier [9,10,11] and will be only briefly recalled here. A Fourier integral transform is applied to the boundary conditions (cf table 1) and to the Lamé equations with correspond to coating and substrate. The transformed equations are then solved. Note that fully adhesive conditions are considered at the interface between coating and substrate.

loading surface	interface	at infinite
at $x = -h$	at $x = 0$	at $x = H$
$\sigma_{xx}^{MC1} = P(y)$ $\sigma_{xy}^{MC1} = 0$	$\sigma_{xx}^{C2} = \sigma_{xx}^{MC1}$ $\sigma_{xy}^{C2} = \sigma_{xy}^{MC1}$ $u^{C2} = u^{MC1}$ $v^{C2} = v^{MC1}$	$\sigma_{xx}^{MC3} = 0$ $\sigma_{xy}^{MC3} = 0$

Table 1 : Boundary conditions for uncracked coating medium

2.3 Crack field σ^F

Displacement discontinuities along crack faces are modelled with continuous dislocation distributions (b_x, b_y) following Dundurs and Mura [12], Faris and Keer [4]. The same technique is used here. Stress and displacement expressions at M are given for a local dislocation situated at D and then for a continuous dislocation distribution.

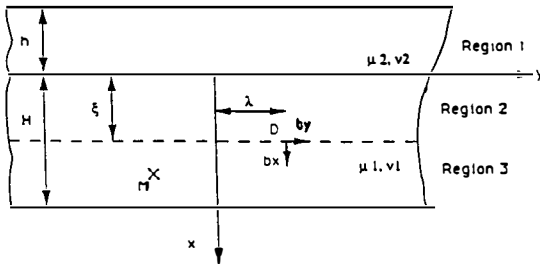


Fig. 1 : Local dislocation diagram

Stresses and displacements generated at M by a local dislocation distribution (b_x, b_y) are obtained from Airy potential functions which respect the boundary conditions expressed in table 2. A Fourier integral transform is applied on the functions and the boundary conditions. The transformed equations are solved in the substrate and in the layer. δ is the Dirac distribution and displacement derivative is made on t variable.

loading surface	interface
at $x = -h$	at $x = 0$
$\sigma_{xx}^F = 0$ $\sigma_{xy}^F = 0$	$\sigma_{xx}^F = \sigma_{xx}^F$ $\sigma_{xy}^F = \sigma_{xy}^F$ $u^F = u^F$ $v^F = v^F$
crack	at infinite
at $x = \xi$	at $x = \gamma$
$\sigma_{xx}^F = \sigma_{xx}^F$ $\sigma_{xy}^F = \sigma_{xy}^F$ $u^F = u^F + b_x \delta(y-\lambda)$ $v^F = v^F + b_y \delta(y-\lambda)$	$\sigma_{xx}^F = 0$ $\sigma_{xy}^F = 0$

Table 2 : Boundary conditions for cracks

δ : Dirac distribution
 $'$: Displacement derivative on t

This leads to:

$$\begin{Bmatrix} \sigma_{xx}^F(x, y) \\ \sigma_{xy}^F(x, y) \\ \sigma_{yy}^F(x, y) \end{Bmatrix} = [M(x, y-\lambda; \xi)] \begin{Bmatrix} b_x(\xi, \lambda) \\ b_y(\xi, \lambda) \end{Bmatrix} \quad (1)$$

$$\begin{Bmatrix} u(x, y) \\ v(x, y) \end{Bmatrix} = [N(x, y-\lambda; \xi)] \begin{Bmatrix} b_x(\xi, \lambda) \\ b_y(\xi, \lambda) \end{Bmatrix} \quad (2)$$

For a continuous dislocation distribution along crack faces, stresses and displacements are:

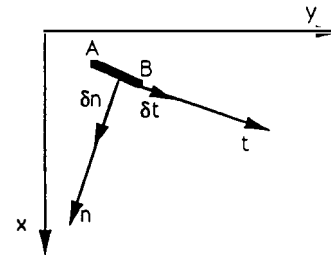


Fig. 2 : Straight crack diagram

$$\begin{Bmatrix} \sigma_{xx}^F(x, y) \\ \sigma_{xy}^F(x, y) \\ \sigma_{yy}^F(x, y) \end{Bmatrix}_{\text{global}} = \int_{\Gamma} [M(x, y-\lambda(t); \xi(t))] \begin{Bmatrix} b_x(\xi(t), \lambda(t)) \\ b_y(\xi(t), \lambda(t)) \end{Bmatrix} dt$$

with $\Gamma = \text{crack}_j$ (3)

No = number of cracks (4)

$$\begin{Bmatrix} u(x, y) \\ v(x, y) \end{Bmatrix} = \int_{\Gamma} [N(x, y-\lambda(t); \xi(t))] \begin{Bmatrix} b_x(\xi(t), \lambda(t)) \\ b_y(\xi(t), \lambda(t)) \end{Bmatrix} dt$$

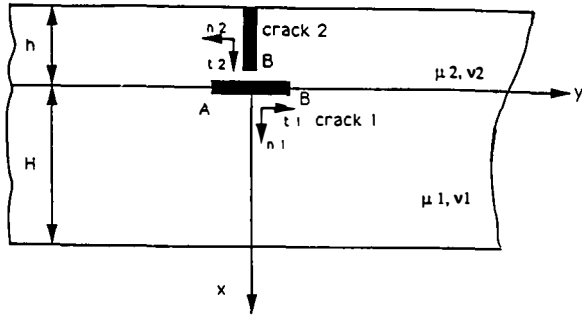


Fig. 3 : Two cracks diagram

When two cracks are present, (cf fig. 3), crack 1 influences crack 2 and vice-versa. Thus stress field (3) turns into (5) as the integration is performed on both cracks. However, the displacement field is not modified as displacements induced by crack 2 impose no relative displacements between crack 1 faces. This leads to:

$$\begin{Bmatrix} \sigma_{xx}^F(x,y) \\ \sigma_{xy}^F(x,y) \\ \sigma_{yy}^F(x,y) \end{Bmatrix}_{\text{global}} = \int_{\Gamma} [M(x,y-\lambda(t); \xi(t))] \begin{Bmatrix} b_x(\xi(t), \lambda(t)) \\ b_y(\xi(t), \lambda(t)) \end{Bmatrix} dt \quad (5)$$

with $\Gamma = \bigcup_{j=1}^{No} \text{crack}_j$
No = crack number

Stresses and displacements for each crack are then expressed in the reference axis of the crack.

$$\begin{Bmatrix} \sigma_{nn}^F(x,y) \\ \sigma_{nt}^F(x,y) \\ \sigma_{tt}^F(x,y) \end{Bmatrix}_{\text{local}} = [\text{Pro}(x,y)] \begin{Bmatrix} \sigma_{xx}^F(x,y) \\ \sigma_{xy}^F(x,y) \\ \sigma_{yy}^F(x,y) \end{Bmatrix}_{\text{global}} \quad (6)$$

$$\begin{Bmatrix} n(x,y) \\ t(x,y) \end{Bmatrix}_{\text{local}} = [\text{Pro}(x,y)] \begin{Bmatrix} u(x,y) \\ v(x,y) \end{Bmatrix}_{\text{global}} \quad (7)$$

System (5) is a system of singular integral Fredholm equations of the second kind where unknowns are complex functions of complex variable $x + iy$. Relation (8) cannot be solved analytically.

$$\gamma B(z) - \frac{\theta}{\pi} v.p \int_{-1}^1 \frac{B_1(t)}{T(t)-z} dt + \sum_{j=1}^{No} \int_{-1}^1 H_1(z-T(t)) B_j(t) dt - H_2(z-T(t)) \bar{B}_j(t) dt = \sigma_1^T(z) - \sigma_1^{MC}(z) \quad (8)$$

with

$$\begin{aligned} i &= 1, No \\ T(t) &= \xi(t) + i \lambda(t) \\ B_1(y) &= b_{y1} - i b_{x1} \\ \sigma^T(y) &= \sigma_{nn}^T + i \sigma_{nt}^T \\ H_1, H_2 &\text{ complex functions of complex variable } \\ \theta, \gamma &\text{ real constant function of } \mu_1, \mu_2, \nu_1, \nu_2 \end{aligned}$$

A numerical solution is found by replacing (8) by an appropriate system of linear equations,

the solution is based on [3]. The fundamental function of the integral equation system (8) is obtained by considering only the dominant part. The fundamental solution for Cauchy type kernels follows that of Muskhelishvili [13]:

$$w_j(t) = (1-t)^{\alpha_j} (1+t)^{\beta_j} \quad |t| \leq 1 \quad (9)$$

$$\alpha_j = \frac{1}{2\pi i} \ln \left(\frac{\gamma+\theta}{\gamma-\theta} \right) + N_j \quad \text{with } N_j \in \mathbb{N} \quad (10)$$

$$\beta_j = -\frac{1}{2\pi i} \ln \left(\frac{\gamma+\theta}{\gamma-\theta} \right) + M_j \quad \text{with } M_j \in \mathbb{N} \quad (11)$$

$$|\text{Re}(\alpha_j)| < 1 \quad |\text{Re}(\beta_j)| < 1 \quad j = 1, \dots, No \quad (12)$$

Thus, the singular nature of the unknown function $B_j(t)$ is characterised by that of the fundamental function $w_j(t)$. Here, the index of this problem (N+M) is -1 or 0. The index is -1 when the crack is embedded: the fundamental function $w(t)$ is therefore singular at both crack tips. The index is 0 when the crack breaks open at the surface, and the fundamental function $w(t)$ is only singular at crack tip B (cf fig. 4).

$B_j(t)$ solution is expressed as a product of a bounded continuous function $\phi_j(t)$ and a fundamental function $w_j(t)$. The unknown function $\phi_j(t)$ can always be represented by an infinite series. This leads to:

$$B_j(t) = w_j(t) \phi_j(t) \quad |t| \leq 1 \quad j = 1, No \quad (13)$$

Observing that $w_j(t)$ is a weight function of Jacobi Polynomials, one may write: (α_j, β_j)

$$B_j(t) = w_j(t) \phi_j(t) = \sum_{n=0}^{\infty} c_{nj} w_j(t) P_n(t) \quad (14)$$

with $c_{nj} = a_{nj} + i b_{nj}$ and $j=1, No$

Displacement expressions are then, according to distribution definition:

$$D_j(s) = - \int_{-1}^s B_j(t) dt \quad (15)$$

with $D_j(s) = \delta_{tj} - i \delta_{nj}$ and $j = 1, No$

Stress and displacement expressions corresponding to the crack response to the load are thus given by relations (8) and (15) respectively. (8) and (15) are linear forms of coordinates c_{nj} . Discretised form of (8) and (15) are presented in chapter 2.4.

2.4 Numerical solution of equations (8) and (15)

B_j serie (14) is then substituted in equation (8), which gives:

$$\sum_{n=0}^{\infty} \gamma w(y) P^{(\alpha, \beta)} - \int_{-1}^1 \left[\frac{\theta c_{n1}}{\pi(T(t)-z)} + \sum_{j=1}^{No} c_{nj} H_1(z-T(t)) \right] w(t) P^{(\alpha, \beta)} dt + \sum_{j=1}^{No} \bar{c}_{nj} \int_{-1}^1 H_2(z-T(t)) \bar{w}(t) P^{(\alpha, \beta)} dt = \sigma^F \quad (16)$$

with $i = 1, No$

Integrals are determined by Gaussian integration. The integration Gaussian points r_i are:

$$P_N(\text{Re}(\alpha_j), \text{Re}(\beta_j)) (r_i) = 0 \quad \begin{matrix} i = 1, \dots, N \\ j = 1, \dots, No \end{matrix} \quad (17)$$

Crack discretisation in N^* observation points s_i transforms linear forms (14) and (15) in 2 N_0 linear systems ($N \times N$) with ($2N \times N_0$) a_{nj} and b_{nj} unknowns, with $c_{nj} = a_{nj} + i b_{nj}$. N is equal to N or $N-1$ for a surface breaking crack or an embedded crack respectively. For an embedded crack, an additional condition is needed to determine the solution. It is provided by crack closure and adherence conditions. Observation points s_i are chosen to be compatible with integration points r_i .

$$P_{N^*}(s_i) = 0 \quad (18)$$

$$j = 1, \dots, N^* \quad j = 1, \dots, N_0$$

Stress and displacement jump expressions due to contact loading are thus available along the whole crack at each observation point s_i . The next step is the contact problem solution along crack faces, i.e. the determination of stick, slip and open zone distribution.

2.5 The contact problem

Distributions of normal and tangential tractions that satisfy the boundary conditions at the crack interface are solved for. These boundary conditions involve equations and inequalities. A systematic approach is thus proposed to avoid assumptions on displacement zone distribution that limit the application field of previous model [6]. The problem is solved as a unilateral contact problem with friction, according to Kalker [14,15] for two body contact. This technique has already been adapted to the crack contact problem by Dubourg and Villechaise [8] and is briefly presented here. The boundary conditions are:

$$\text{open zone: } \sigma_{nn}^T = 0 \quad \delta_n > 0 \quad (19)$$

$$\sigma_{nt}^T = 0$$

$$\text{stick zone: } \delta_n = 0 \quad \sigma_{nn}^T < 0 \quad (20)$$

$$\delta_t = 0 \quad |\sigma_{nt}^T| < f |\sigma_{nn}^T|$$

$$\text{slip zone: } \delta_n = 0 \quad \sigma_{nn}^T < 0 \quad (21)$$

$$|\sigma_{nt}^T| = f |\sigma_{nn}^T| \quad \sigma_{nt}^T \cdot \delta_t > 0$$

An iterative process is used. For the initial state, the crack is assumed to be in contact and adherent. System of equations (15) and (16) with the corresponding boundary conditions are solved for. Then the status of each points (stick, slip and open) is tested by checking the corresponding inequalities. If a condition is not satisfied, the status of the point is altered, and systems (15) and (16) are solved again. This goes on until a stable distribution of stick, slip and open zones is obtained.

2.6 Stress intensity factor K and elastic energy release rate G

Stresses and relative displacements are obtained. It is thus possible to determine the complex stress intensity factor K and the energy release rate G. The factor K (SIF) represents the stress field singularity at the crack tips, according to [3].

at tip B:

$$K_{Re} + iK_{Im} = \lim_{t \rightarrow 1} (t-1)^{-\alpha} (t+1)^{-\beta} (\sigma_{nn} + i\sigma_{nt}) \quad (22)$$

at tip A:

$$K_{Re} + iK_{Im} = \lim_{t \rightarrow -1} (1-t)^{-\alpha} (-t-1)^{-\beta} (\sigma_{nn} + i\sigma_{nt}) \quad (23)$$

For a crack situated in an homogeneous medium, real and imaginary parts of the SIF K correspond respectively to mode I and mode II. This definition is no longer valid on for interfacial crack [5] and the energy release rate G is used. Thus [2]:

$$G = - \frac{1}{4\theta} |K|^2 \quad (24)$$

2.7 Conclusion

The energy release rate G is determined for straight cracks situated at the interface of a coating medium and normal at its interface. Cracks are modelled with continuous dislocation distributions. Fourier transforms are used to obtain stress and displacement expressions versus dislocation distributions. Displacement zone distribution along crack faces that govern G is determined by solving the contact problem as an unilateral contact problem with friction.

3. Real Cases

Two modes of coating failure are observed [7]. They result from crack propagation (cf fig. 4 and 5). Spall detachment comes either from (cf fig. 4 and 5):

- interfacial cracks that propagate at the interface and finally meet a crack normal to the surface
- or a crack that propagates perpendicular to the surface and meets an interfacial crack.

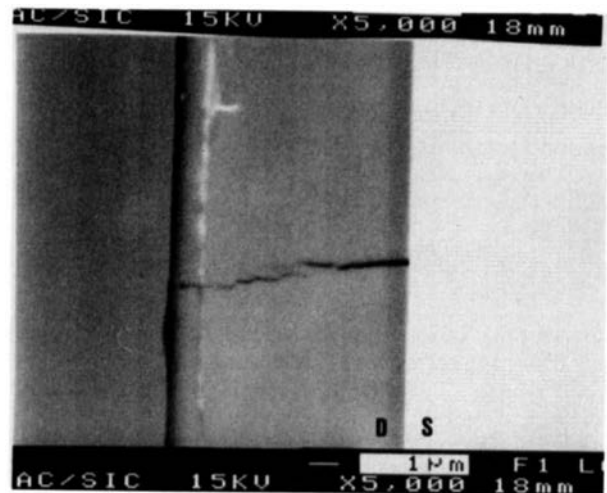


Fig. 4 : Crack configuration leading to spall detachment [7]

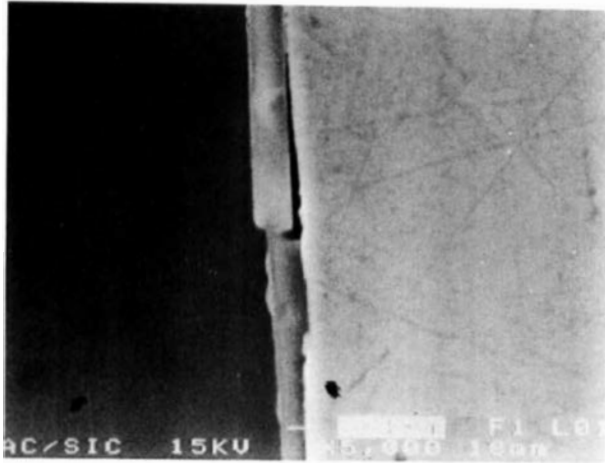


Fig. 5 : Spall detachment [7]

This typical configuration shown in figure 5 is modelled in the next part to better the understanding of the coating failure process.

4. Application

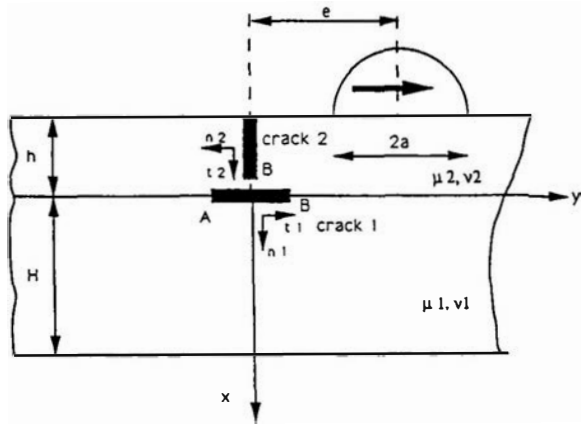


Fig. 6 : Configuration diagram

The configuration studied is presented in figure 6. The substrate is steel and the 80 μm thick coating is TiN. Mechanical characteristics are presented below:

	Young's modulus	Poisson's ratio
coating: TiN	600 GPa	0.34
substrat: steel	210 GPa	0.3

The hertzian load moves from left to right. Loading parameters are:

load C_n	211 kN/m
Radius of cylinder punch R	22 mm

For the steel half plane, these conditions produce a maximum hertzian pressure p_0 of 840 MPa and a contact size $2a = 0.320$ mm. Two questions must be answered:

- does mutual crack interaction favour crack propagation ?
- what is the effect of crack length on propagation ?

4.1 Influence of crack interactions

Cracks behave differently in multiple than in single crack systems, G variations are modified. Influence of crack 2 on crack 1 is thus studied (cf fig. 7 and 8). G variations at both tips A and B of crack 1 versus e/a are presented below in the "reference case" when crack 1 is alone and in the "interaction case" when both cracks are present. Crack length is held constant, 70 μm for crack 1 and 75 μm for crack 2.

The two maxima observed come from the two extrema of the interfacial shear stress [7], situated at the edges of the contact loading zone. The interaction domain, or domain within which crack interaction is significant, is varying from $e/a = -1$ to $e/a = 1$. The interaction level is characterised by the percentage change in G reference brought about by the presence of the other crack. Interactions vary from -61% to 78% for tip A and from 0% to 53% for tip B. A negative or positive values correspond respectively to a decrease and an increase of rate G . Therefore, the influence of crack 2 on crack 1 is harmful or beneficial at tip A and always harmful at tip B.

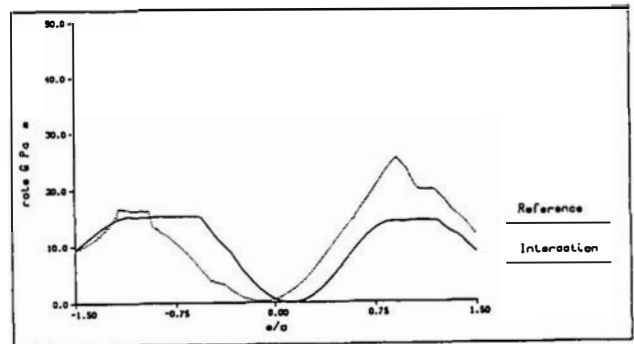


Fig. 7 : Energy release rate G at tip A of crack 1

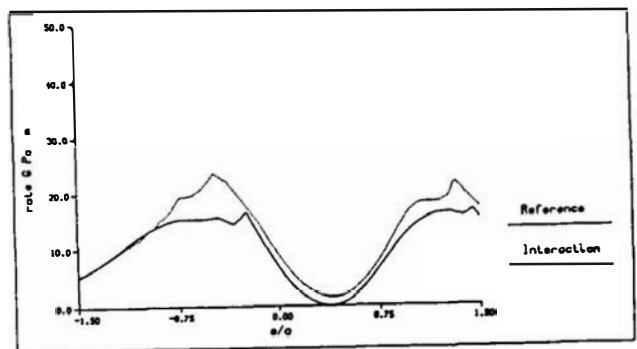


Fig. 8 : Energy release rate G at tip B of crack 1

Interactions are therefore far from negligible. The same conclusions are drawn concerning the influence of crack 1 on crack 2. Multiple cracks must be analysed simultaneously. The influence of crack length is studied now in a two crack system.

4.2 Influence of length of crack 1 and 2

The variation of G at crack tip B of crack 2 and at crack tips A and B of crack 1 is first studied versus e/a for various lengths of crack 1. The length of crack 2 is held constant and equal to $75 \mu\text{m}$ (cf fig. 9). The same problem is solved for various lengths of crack 2, when the length of crack 1 is held constant and equal to $70 \mu\text{m}$ (cf fig. 10). The figures 9 and 10 are presented in the appendix. The different crack lengths considered are:

crack 1 : 50, 60, 70, 80 μm

crack 2 : 60, 70, 75 μm

Results show that:

- Influence of the length of crack 1 on G at:

tip A of crack 1 (fig 9a): G increases with increasing length of crack 1.

tip B of crack 1 (fig 9b): G decreases with increasing length of crack 1.

tip B of crack 2 (fig 9c): G decreases lightly for the first maximum and increases for the second maximum with increasing length of crack 1.

- Influence of the length of crack 2 on G at:

tip A of crack 1 (fig 10a): G increases with increasing length of crack 2.

tip B of crack 1 (fig 10b): G decreases with increasing length of crack 2.

tip B of crack 2 (fig 10c): G decreases for the first maximum and increases for the second maximum with increasing length of crack 1.

Further an increase in length of cracks 1 and 2 causes an increase of G at tip A and B of crack 1.

These results suggest the following spall detachment process:

- crack 2 propagation down to the interface is feasible.

- crack 1 propagation is feasible at tip A and tip B. But as G values are more important at tip A than at tip B, propagation is favoured at tip A, in an opposite direction with respect to the load displacement direction.

This analysis is only qualitative, as failure criteria and propagation laws for interfacial cracks and cracks in coating are lacking. A failure criterion could for exemple be a boundary on complex plan K as suggested by to Rice and Sih [16].

5 Conclusion

A cracked layered medium was used to study the conditions that lead to spall detachment. The model is half-analytical and half-numerical. It gives good accuracy and requires short computer times. A configuration taken from experiments was studied. The spall detachment may proceed as follows:

- propagation of normal crack down to the interface,

- propagation of interfacial crack in the opposite direction of the load displacement.

Rupture criteria are only established for uncoated cracked half-plane. Criteria are thus needed for interfacial and normal cracks in cracked coated media.

Références

[1] ERDOGAN F., GUPTA G., The stress analysis of multi-layered composites with flaw, Int. J. Solids structures, 1971, Vol 7, p 39-61

[2] ERDOGAN F., GUPTA G., Layered composites with an interface flaw, Int. J. Solids structures, 1971, Vol 7, p 1089-1107

[3] ERDOGAN F., GUPTA G., Methods of analysis and solutions of crack problems, Mechanics of fracture 1, SIH G.C., Noordhoff international publishing, Leyden, 1973, p 368-425, ISBN 90 01 79860 8

[4] FARRIS T.N., KEER L.M., Williams' Blister test analyzed as an interface crack problem, International journal of fracture, 1985, Vol 27, p 91-103

[5] RICE J.R., Elastic fracture mechanics concepts for interfacial cracks, Journal of applied mechanics, Vol. 55, 1988, p 98-103

[6] KIM S.H., KEER L.M., CHENG H.S., Loss of adhesion of a layer bonded to an elastic half space caused by a concentrated contact, 1990, Vol. 53, p 53-59

[7] IGNAT M., Private communication, Laboratoire de thermodynamique et physico-chimie métallurgiques, URA 29

[8] DUBOURG M. C., VILLECHAISE B., Unilateral contact analysis of a crack with friction, Eur. J. Mech. A/Solids, 1989, Vol. 8, n°4, p 309-319

[9] LEROY J.M., Modélisation thermoélastique des revêtements de surface utilisés dans les contacts non lubrifiés, Thèse : Institut National des Sciences Appliquées de Lyon, 1989, 210 p

[10] LEROY J.M., FLOQUET A., VILLECHAISE B., Thermomechanical behavior of multilayered media: Theory, Journal of applied mechanics, 1989, Vol. 111, p 538-544

[11] LEROY J.M., FLOQUET A., VILLECHAISE B., Thermomechanical behavior of multilayered media: Results, Journal of applied mechanics, 1990, Vol. 112, p 317-323

[12] DUNDURS J., MURA T. Interaction between an edge dislocation and circular inclusion, J. Mech. Phys. Solids, 1964, Vol. 12, p 177-183

[13] MUSHKHELISHVILI N.I., Singular integral equations, Noordhoff international publishing : Leyden, 1977, 144p, ISBN 90 60700 4

[14] KALKER J. J., The contact between wheel and rail, Reports of the departement of mathematics and informatics, 1982 a, Delft

[15] KALKER J. J., Two algorithms for the contact problem in elastostatic. Reports of the departement of mathematics and informatics, 1982 b, Delft

[16] RICE J. R., SIH G. C., Plane problems of cracks in dissimilar media, J. of Applied Mech., 1965, p 418-423

Appendix

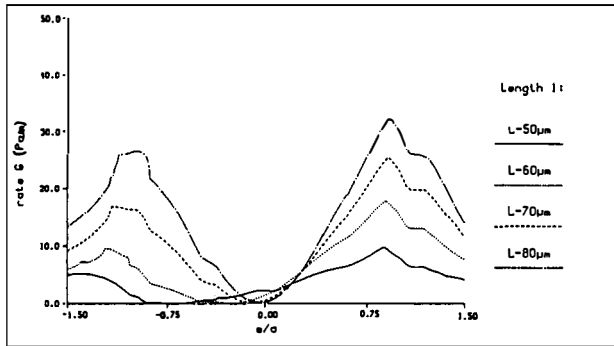


Fig. 9a : Energy release rate G at tip A of crack 1

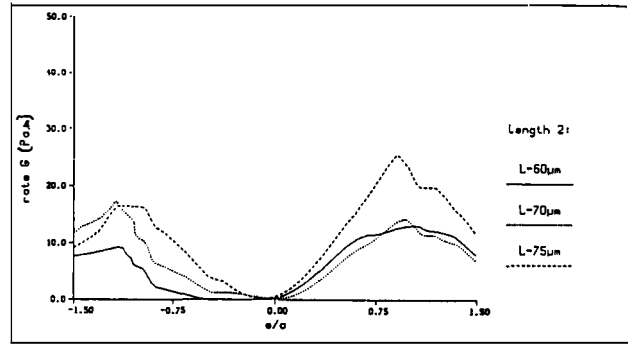


Fig. 10a : Energy release rate G at tip A of crack 1

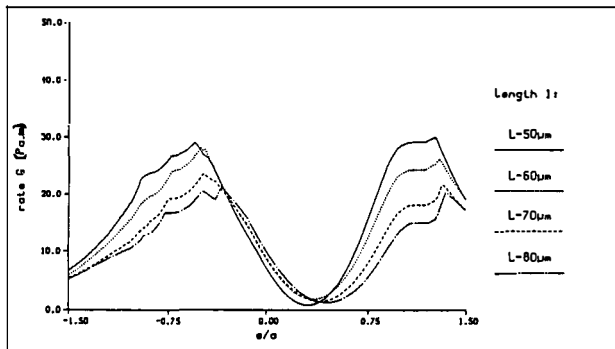


Fig. 9b : Energy release rate G at tip B of crack 1

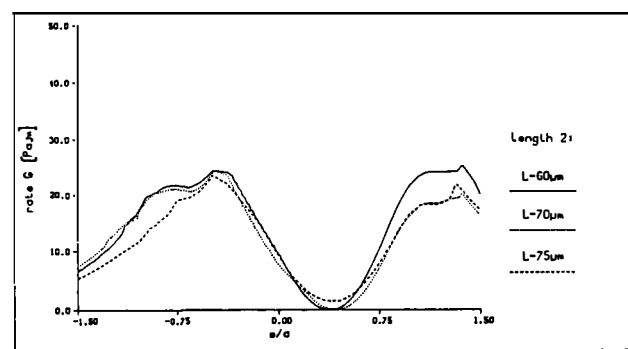


Fig. 10b : Energy release rate G at tip B of crack 1

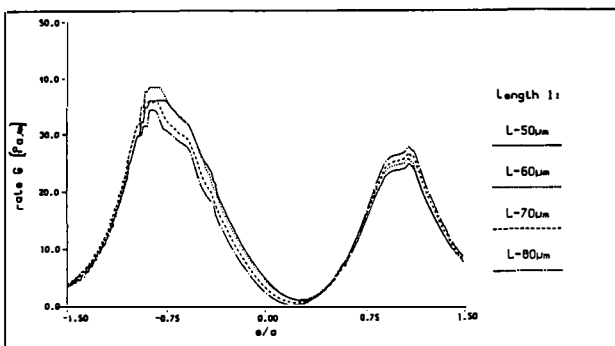


Fig. 9c : Energy release rate G at tip B of crack 2
 Fig. 9 : Energy release rate G for couple TiN/steel

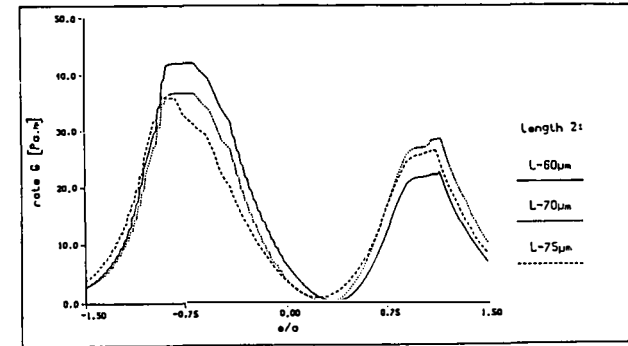


Fig. 10c : Energy release rate G at tip B of crack 2
 Fig. 10 : Energy release rate G for couple TiN/steel